Perilipin membrane integration determines lipid droplet heterogeneity in differentiating adipocytes

Mario Majchrzak, Ozren Stojanović, Dalila Ajjaji, Kalthoum Ben M'barek, Mohyeddine Omrane, Abdou Rachid Thiam, Robin Klemm

Cell Reports

Report

Perilipin membrane integration determines lipid droplet heterogeneity in differentiating adipocytes

Graphical abstract

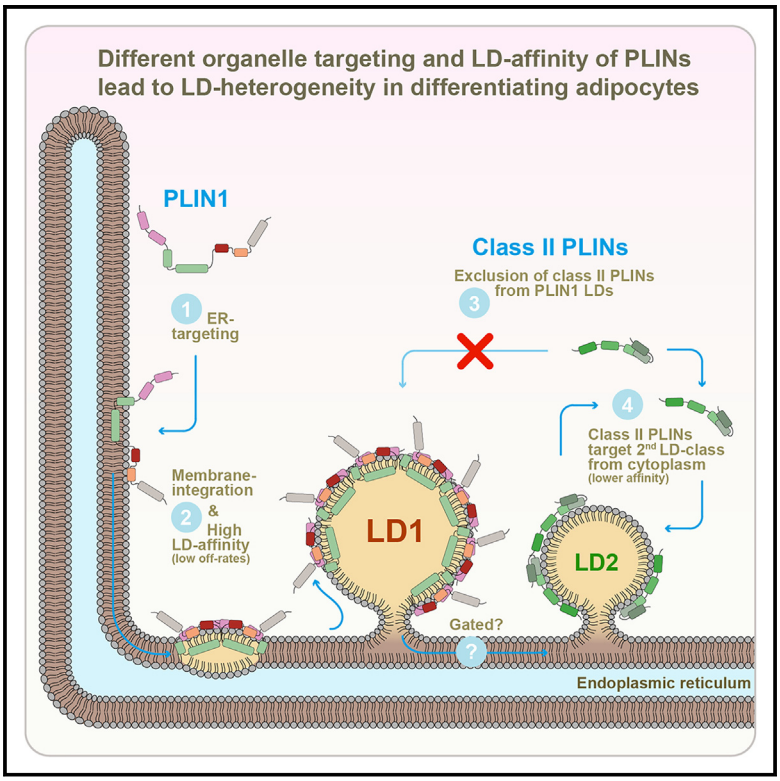

Highlights

- PLIN1 is an integral membrane protein behaving as a class I LD protein
- An unconventional integral membrane segment (iMS) mediates ER insertion
- High-affinity LD binding by the iMS excludes class II PLINs from PLIN1 LDs
- PLIN1 movement between the LDs and the ER is likely a gated process

Authors

Mario Majchrzak, Ozren Stojanović, Dalila Ajjaji, Kalthoum Ben M'barek, Mohyeddine Omrane, Abdou Rachid Thiam, Robin W. Klemm

Correspondence

robin.klemm@dpag.ox.ac.uk

In brief

Majchrzak et al. use biochemistry, fluorescence microscopy, and *in vitro* experiments to identify molecular features in PLIN1 that determine lipid droplet heterogeneity in differentiating adipocytes. ER insertion and high lipid droplet affinity are key properties of PLIN1 leading to the formation of distinct LD populations upon acute fatty acid uptake.

Majchrzak et al., 2024, Cell Reports *43*, 114093
April 23, 2024
https://doi.org/10.1016/j.celrep.2024.114093

CellPress

Cell Reports

CellPress
OPEN ACCESS

Report

Perilipin membrane integration determines lipid droplet heterogeneity in differentiating adipocytes

Mario Majchrzak,[2] Ozren Stojanović,[1] Dalila Ajjaji,[3] Kalthoum Ben M'barek,[3] Mohyeddine Omrane,[3] Abdou Rachid Thiam,[3] and Robin W. Klemm[1,2,4,*]

[1]Department of Physiology, Anatomy, and Genetics, University of Oxford, Oxford OX1 3PT, UK
[2]Department of Molecular Life Sciences, University of Zurich, 8057 Zurich, Switzerland
[3]Laboratoire de Physique de l'École Normale Supérieure (ENS), Université PSL, CNRS, Sorbonne Université, Université de Paris, 75005 Paris, France
[4]Lead contact
*Correspondence: robin.klemm@dpag.ox.ac.uk
https://doi.org/10.1016/j.celrep.2024.114093

SUMMARY

The storage of fat within lipid droplets (LDs) of adipocytes is critical for whole-body health. Acute fatty acid (FA) uptake by differentiating adipocytes leads to the formation of at least two LD classes marked by distinct perilipins (PLINs). How this LD heterogeneity arises is an important yet unresolved cell biological problem. Here, we show that an unconventional integral membrane segment (iMS) targets the adipocyte specific LD surface factor PLIN1 to the endoplasmic reticulum (ER) and facilitates high-affinity binding to the first LD class. The other PLINs remain largely excluded from these LDs until FA influx recruits them to a second LD population. Preventing ER targeting turns PLIN1 into a soluble, cytoplasmic LD protein, reduces its LD affinity, and switches its LD class specificity. Conversely, moving the iMS to PLIN2 leads to ER insertion and formation of a separate LD class. Our results shed light on how differences in organelle targeting and disparities in lipid affinity of LD surface factors contribute to formation of LD heterogeneity.

INTRODUCTION

Adipocytes deposit an excess of dietary nutrients as triacylglycerols (TAGs) in large lipid droplets (LDs) and release fatty acids to feed other tissues during fasting.[1–3] Deficiencies in LD biogenesis and turnover are associated with several metabolic diseases, such as lipodystrophies, fatty liver disease, type 2 diabetes, and obesity.[4–6]

LDs form at the membranes of the endoplasmic reticulum (ER) when neutral lipids, such as TAGs, accumulate between the two leaflets of the lipid bilayer.[7–9] When TAG amounts increase, they phase separate and form lenses, which eventually bud out into the cytoplasm as LDs. The LD surface is surrounded by a phospholipid monolayer and specific surface proteins.[10–15]

In principle, all LDs within a cell should have the same lipid and protein composition. Accumulating evidence suggests, however, that LDs are highly heterogeneous and can specialize into different sub-populations that are morphologically, chemically, and functionally distinct.[14,16–22]

One way by which cells can generate different LD classes is through the synthesis of specific hydrophobic cores. For example, fly fat bodies contain a population of large LDs, which is mostly filled with TAGs derived from *de novo* lipogenesis.[23,24] A class of smaller LDs in the periphery of the cell seems to store TAGs made preferentially from dietary fatty acids (FAs).[23,24] Consistent with these findings, FA feeding of mammalian adipocytes leads to the formation of distinct LD classes.[10,25,26] A central LD population is formed mainly by *de novo* lipogenesis,[27] whereas acute FA influx triggers the formation of a second, peripheral LD class.[10,25,26] The mechanisms that lead to the formation of different LD populations remain, however, poorly understood, and it is largely unclear how LD surface factors can be targeted to separate LD populations in the cell.

In general, protein targeting to LDs occurs by two major pathways.[14,28,29] Class I proteins are synthesized as monotopic integral membrane proteins at the ER and subsequently move to the LD surface using the ERTOLD (ER to LD targeting) pathway (Figure 1A, class I). The dual localization to the ER and the LDs is facilitated by special membrane anchors that often fold into hairpins.[13,29]

Class II or CYTOLD (cytoplasm to LD targeting) proteins, on the other hand, bind LDs directly from the cytoplasm (Figure 1A, class II). They do not possess integral membrane segments and are instead targeted to the LD by amphipathic domains detecting packing defects in the LD monolayer where the hydrophobic LD core is exposed.[14,30–35]

The perilipins (PLINs) are currently viewed as prototypical class II proteins, comprising a family of evolutionarily conserved LD surface factors carrying out important structural and regulatory functions.[26,36–39] The family defining amphipathic PAT

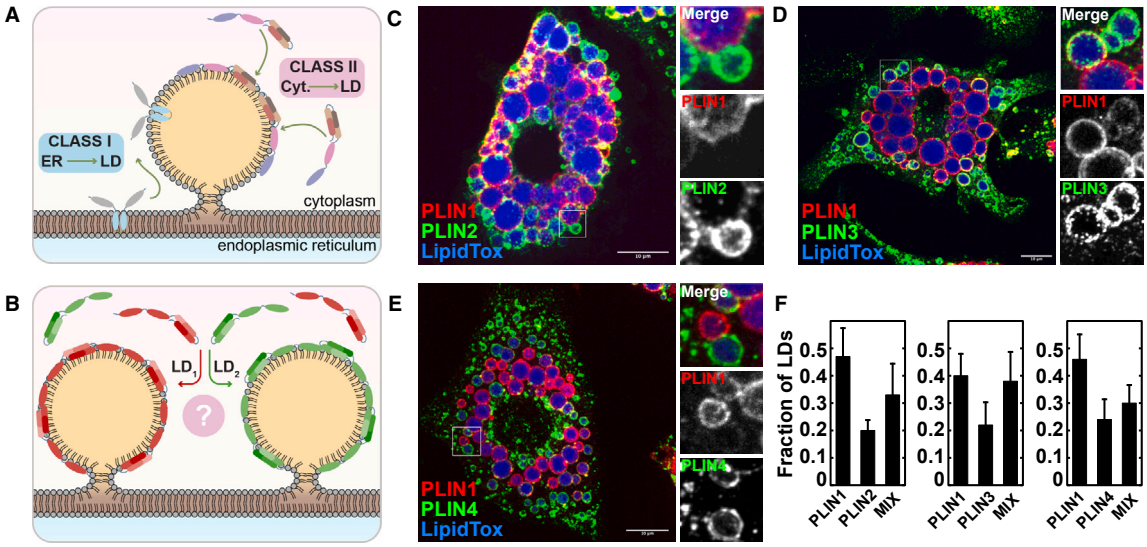

Figure 1. FA feeding leads to the formation of at least two distinct LD classes in adipocytes

(A) Class I LD proteins move from the ER to the LD surface. Class II LD proteins bind to LDs directly from the cytoplasm.

(B) Segregation of class II proteins to different LD classes.

(C) Day 6 3T3-L1 adipocytes fed with 750 μM Na^{2+}oleate for 3 h. Endogenously expressed PLIN1 and PLIN2 were visualized by immunofluorescence. Scale bar, 10 μm.

(D) As in (C), but PLIN1 and PLIN3 were imaged.

(E) As in (C), but PLIN1 and PLIN4 were imaged.

(F) Quantification of the results in (C)–(E). $n = 9$, $n = 9$, and $n = 8$ cells, for co-staining with PLIN1 and PLIN2, or PLIN1 and PLIN3, or PLIN1 and PLIN4, respectively. Fraction of LDs marked by both perilipins labeled as "MIX." LD counts per replicate, >100; values are means of fraction of LD covered by either or both perilipins in each cell ± SEM.

See also Figure S1.

domain and the following 11-mers mediate LD targeting (Figure S1A).[32,37,40,41] The PLINs are all thought to target the LD from the cytoplasm and should therefore mix on the same LD class. The LD sub-populations that form in differentiating adipocytes upon FA feeding are, however, marked by specific PLINs (Figure 1B).[10,25,26] An affinity-based LD binding "hierarchy" among the different PLIN family members is likely key to the formation of the two LD classes.[34,40,42–45] However, the biochemical characterization of the responsible targeting domains remains incomplete.[38]

RESULTS

Acute FA feeding induces the formation of distinct LDs in adipocytes

To investigate PLIN targeting to LDs, we differentiated 3T3-L1 cells into white adipocytes and visualized endogenously expressed PLIN1, PLIN2, PLIN3, and PLIN4 after FA feeding by immunofluorescence (PLIN5 is not expressed in 3T3-L1 adipocytes[11,27]). Confirming previous observations,[26,36,39,40,42] we observed distinct LD populations (Figures 1B–1F). A central LD class was almost exclusively labeled with PLIN1, and a second, peripheral population was marked by PLIN2, PLIN3, and PLIN4 (Figures 1C–1E). The second population was either exclusively marked by PLIN2, PLIN3, and PLIN4 or contained sometimes low amounts of PLIN1, which we called mixed LDs (Figures 1C–1E, magnifications, and 1F, MIX).

Consistent with our results in adipocytes and the established LD binding hierarchy,[26,43] we next showed that ectopically expressed PLIN1 excluded PLIN2, PLIN3, or PLIN4 from LDs when co-transfected in COS7 cells (Figures S1A–S1D). This behavior was dependent on features C-terminally of the 11-mer domain (Figure S1A). A construct only consisting of the N-terminal PAT and 11-mer regions (PLIN1 1–192) mixed well with PLIN2 on the LD surface (Figure S1E).

Together, these data raised the question of how class II LD proteins can separate onto different LD populations.

PLIN1 is an integral membrane protein dually localizing to the ER and LDs

To determine the molecular basis of PLIN LD targeting, we expressed PLIN1 and 2 in COS7 cells. As expected, PLIN1 localized to the endogenous LDs but was, surprisingly, never seen in the cytoplasm. Instead, it always bound to the ER (Figures 2A and S2B). Consistent with previous work,[45] these data indicated that PLIN1 is not a prototypical class II LD protein. On the other hand, PLIN2 showed normal class II behavior, accumulating in the cytoplasm upon overexpression and covering all endogenous LDs (Figures 2B, S2A, and S2D). After addition of FA (Na^+ oleate), both PLIN1 and PLIN2 targeted efficiently to LDs (Figures 2C–2E).

Since PLIN1 does not contain any predicted membrane segments (Figures S2D and S2E) and exhibits similar overall hydrophobicity as PLIN2 (Figures S2F and S2G), we initially expected it to bind the ER as a peripheral membrane protein, perhaps

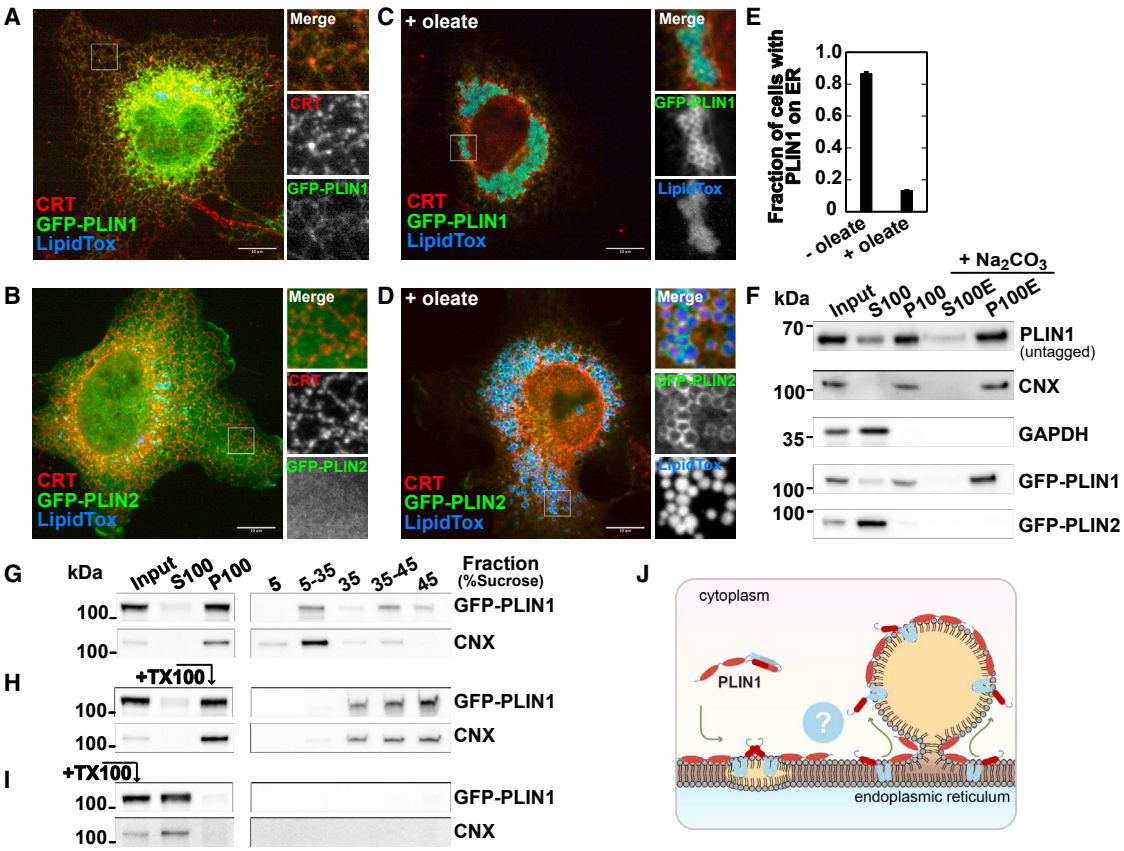

Figure 2. PLIN1 is an integral membrane protein that localizes to the ER and LDs

(A) GFP-murine PLIN1 was expressed in COS7 cells. The ER is visualized with an antibody against calreticulin (CRT). LDs are stained with LipidToxRed. Scale bar, 10 μm.

(B) As in (A), but the cells expressed GFP-PLIN2.

(C) As in (A) but with 250 μM Na^+ oleate for 6 h.

(D) As in (C), but the cells expressed GFP-PLIN2.

(E) Quantification of results in (A) and (C) with GFP-PLIN1 on the ER. $n = 3$ independent experiments with >1,500 cell per replicate; fraction of PLIN1 on the ER ± SD.

(F) COS7 cells expressing untagged PLIN1, GFP-PLIN1, or GFP-PLIN2 were fractionated, followed by alkaline extraction. Input is cell lysate; S100 is supernatant and P100 pellet of a 100,000 × *g* centrifugation, S100E and P100E denote the same after alkaline (Na_2CO_3) extraction. GAPDH, glyceraldehyde 3-phosphate dehydrogenase; CNX, calnexin.

(G) As in (F), but P100 was floated on a sucrose step gradient.

(H) As in (G), but P100 was incubated with Triton X-100 before flotation.

(I) As in (H), but the cell lysate was treated with Triton X-100 before centrifugation.

(J) PLIN1 is an integral membrane protein with a membrane anchor (blue) allowing ER and LD targeting.

See also Figure S2.

through a receptor. In support of this view, PLIN1 sedimented together with the endogenously expressed integral ER protein calnexin (CNX) to the membrane pellet (Figure 2F, PLIN1 untagged, GFP-PLIN1, P100).

However, when we subjected the membrane pellet to alkaline extraction with Na_2CO_3 buffer, PLIN1 remained in the alkali-resistant membrane fraction (Figure 2F, P100E), behaving like an integral membrane protein. PLIN2 co-fractionated with the soluble cytoplasmic marker glyceraldehyde 3-phosphate dehydrogenase (GAPDH; Figure 2F, S100).

To exclude possible artifacts, we carried out flotation experiments with a ribosome-stripped membrane fraction from cells expressing PLIN1. Figure 2G shows that PLIN1 moved efficiently out of the bottom fraction and floated on a sucrose step gradient together with ER membranes marked by CNX (5%–35% sucrose interface). Addition of detergent to P100 prevented flotation (Figure 2H), and PLIN1 and CNX both remained soluble when we mixed the cell lysate with detergent before high-speed centrifugation (Figure 2I).

Taken together, our data indicated that PLIN1 does not belong to the cytoplasmic class II proteins. As an integral membrane protein, it might move from the ER to the LD surface. Indeed, we found that the PLIN1 ER pool re-distributed efficiently to LDs when we blocked translation with cycloheximide for 1 h before LD induction by FA feeding (Figures S2H–S2J).

PLIN1 contains an unconventional integral membrane segment and a peripheral membrane binding motif

We next aimed to identify the domains necessary for PLIN1 membrane integration. We therefore carried out a systematic structure-function analysis using fluorescence microscopy and subcellular fractionation followed by alkaline extraction as parallel readouts.

We started with a minimal N terminus of the mouse PLIN1 sequence (PLIN1 1–192) containing the PAT-domain (acronym perilipin/ADRP/TIP47, former names for PLIN1/2/3) and 11-mer regions, which are sufficient for LD targeting (Figure S3A).[32,40,43] As expected, neither of these two domains, nor a polybasic region enriched in prolines downstream of the 11-mer region, was involved in ER targeting. The N-terminal PLIN1 portion until position 237 remained completely soluble (Figure 3A, S100) localizing to the cytoplasm and the endogenous LDs (Figures 3B and S3B).

However, a construct extended until residue 281 (PLIN1 1–281) pelleted efficiently to the membrane fraction and was alkali resistant (Figure 3A, P100E). Since it localized to the ER, as determined by microscopy, the region between residues 238 and 280 likely contained an integral membrane segment (iMS) (Figures 3A, green domain, and S3B). Interestingly, the corresponding C-terminal portion (PLIN1 281–517) was found in the supernatant S100 (Figure 3A) but localized to the ER, as shown by microscopy (Figure 3D), suggesting that PLIN1 contains an additional peripheral membrane segment (pMS) contributing to ER binding. Computational analysis of the C-terminal portion predicted a strong amphipathic region between residues 380 and 400 (Figure 3A, yellow). However, a construct containing this motif (PLIN1 371–517) remained completely soluble (Figures 3A and 3E). Further extension of the C-terminal part until the beginning of the 4-helix bundle (PLIN1 328–517) led to ER localization (Figure 3F), but this construct remained soluble in the fractionation experiments (Figure 3A), indicating that the potential pMS is positioned in this section of the middle domain (Figure 3A, orange).

To narrow down the two membrane binding regions further, we turned to hydropathy plot analysis (Figure S2F). A first segment with moderate hydrophobicity was found between tryptophan 238 and proline 280 of the mouse PLIN1 sequence, corresponding to the region in which we identified the iMS (Figures S2F and 3G). A second region with moderate hydrophobicity between residues 348 and 370 overlapped with the pMS (Figures S2F and 3G).

To test the function of these domains in ER targeting, we deleted them. PLIN1ΔΔ lacking both the iMS and the pMS (Figure 3G, PLIN1 Δ238–280, Δ348–370) was completely soluble and did not float (Figure 3H). Additionally, this mutant localized to the cytoplasm (Figure 3I). Although having lost its ability to bind the ER, PLIN1ΔΔ was still found on LDs after FA feeding and now often mixed with PLIN2 (Figure 3J). In conclusion, removal of the iMS and the pMS converted PLIN1 into a class II LD protein, targeting LDs directly from the cytoplasm (Figure 3K).

In agreement with this model, addition of the iMS to PLIN2, right downstream of the 11-mer region (PLIN2-iMS, insertion at position 251), was sufficient for membrane integration (Figures S3C–S3E). ER insertion of PLIN2-iMS permitted efficient competition with PLIN1 for LD formation at the ER (Figure S3E). However, in contrast to our expectation, PLIN2-iMS did not mix with PLIN1 on the same LDs but tended to segregate onto a separate LD class (Figure S3E), indicating a critical function for the iMS in the nucleation of different LD populations at the ER.

Taken together, our data show that PLIN1 behaves as an integral ER membrane protein, showing characteristics of a class I rather than a class II LD protein. Both the iMS and the pMS are sufficient for ER targeting, but membrane integration and the generation of different LD classes depend on the iMS. Removing the ability to integrate into the ER converts PLIN1 into a conventional class II LD protein. The ER binding-deficient PLIN1 mutant mixes better with class II PLINs on the same LDs, indicating that it has reduced LD affinity.

The iMS is critical in determining PLIN1 LD binding kinetics

To investigate this possibility, we analyzed the monolayer affinity of PLIN1 and PLIN1ΔΔ *in vitro* (Figure 4A).[31] Shrinkage of the aqueous compartments in a buffer-in-oil system leads to compression of an artificial LD monolayer at the oil-buffer interface. The proteins fall off the monolayer with progressive reduction of the interface area and accumulate proportionally to their off-rates in the buffer compartment.[31] In agreement with the microscopy and fractionation experiments (Figures 3G–3K),[40,42] full-length PLIN1 remained efficiently bound to the interface of the buffer compartment, indicating that the high LD affinity is determined by low off-rates from the monolayer (Figure 4B). In comparison, PLIN1ΔΔ was readily released from the interface, showing faster off-rates and, thus, lower affinity (Figures 4A and 4B). The progressive accumulation in the buffer phase showed that PLIN1 excluded PLIN1ΔΔ from the LD surface mimic, confirming the results in cells (Figures 4A and 4B).

To gain insights into the corresponding on-reaction of the binding equilibrium, we used fluorescence recovery after photobleaching. Deletion of either the iMS (PLIN1ΔiMS) alone or together with the pMS (PLIN1ΔΔ) made recovery on the LD faster by more than an order of magnitude compared to a mutant in which the iMS is present and only the pMS is removed (PLIN1ΔpMS) (Figure 4C and still frames in Figure S4A).

Together, these results suggest that PLIN1 binds LDs with low off- and on-rates, which is determined by the iMS. LD binding via the classical amphipathic segments appears to be faster but occurs with lower LD affinity.

These data suggested that differences in membrane targeting and LD affinity by the PLINs may provide part of the mechanisms by which LD heterogeneity arises in adipocytes: PLIN1 is targeted to the ER via the iMS, where it binds to the emerging LDs with high affinity, excluding the low-affinity PLINs. However, because PLIN1 is kinetically trapped on this first LD population, it cannot immediately bind to the second LD class, which emerges upon FA feeding. At this stage, PLIN2, PLIN3, and PLIN4 can readily bind to the surface of the acutely synthesized LDs from the cytoplasm. Despite their lower LD affinity, the class II PLINs label the second LD population first.

CellPress
OPEN ACCESS

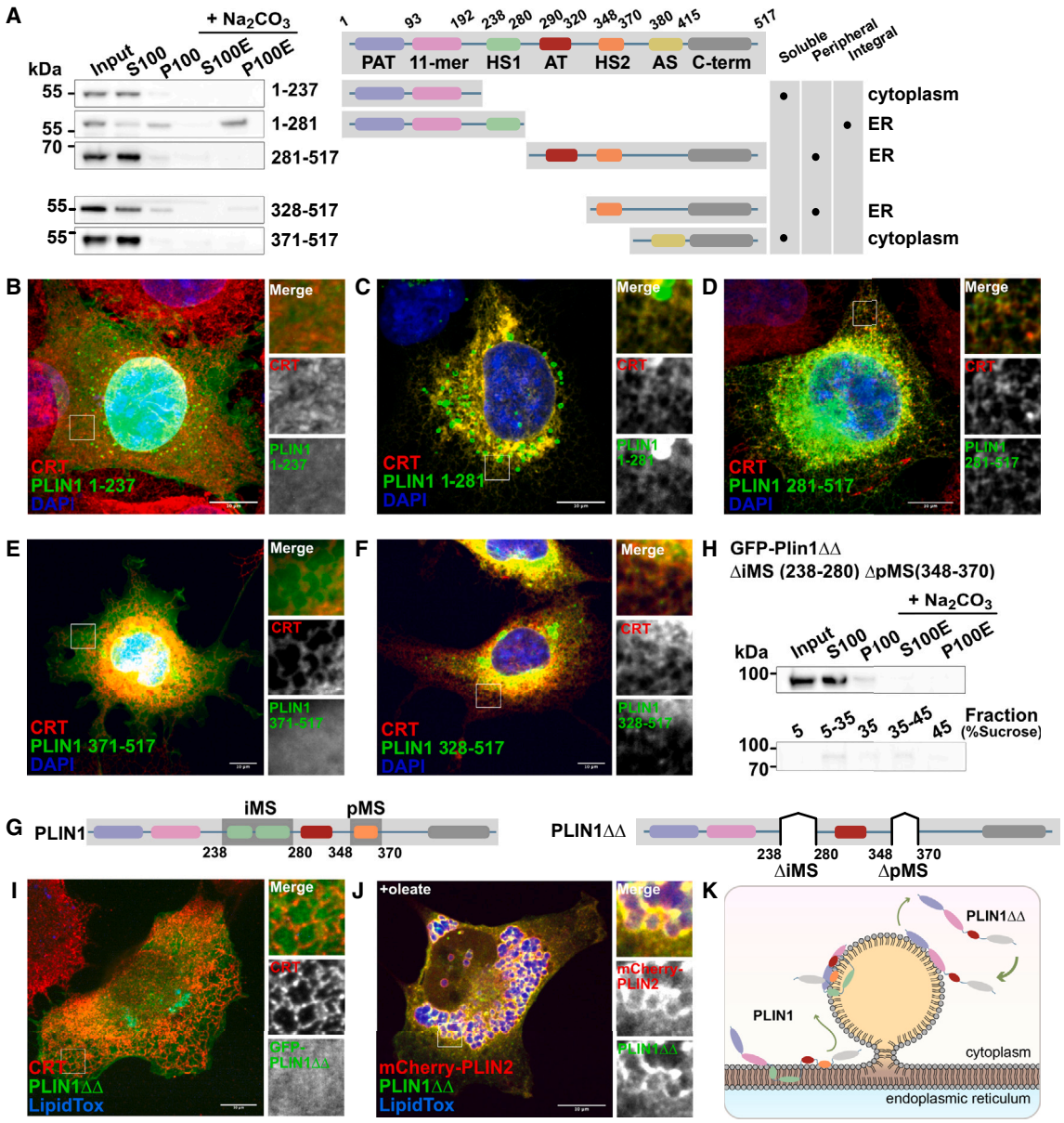

Figure 3. Identification of two ER-targeting segments in PLIN1

(A) PLIN1 analysis by fractionation and alkaline extraction and western blotting with an anti-GFP antibody. See Figure S3 for domain description.

(B) COS7 cells expressing GFP-PLIN1 (1–237). The ER was visualized with an antibody to CRT. The nuclei were stained with DAPI. Scale bar, 10 μm.

(C) As in (B) but with PLIN1 1–281.

(D) As in (B) but with PLIN1 281–519.

(E) As in (D) but with PLIN1 371–517.

(F) As in (D) but with PLIN1 328–517.

(G) Illustration of the integral membrane segment (iMS; 238–280) and the peripheral membrane segment (pMS; 348–370) and PLIN1ΔΔ lacking both.

(H) As in (A) but deletion of iMS and pMS (GFP-PLIN1ΔΔ). P100 was subjected to alkaline extraction (+Na_2CO_3) and floated.

(I) As in (B) but with PLIN1ΔΔ. LDs were stained with LipidToxDeepRed.

(J) COS7 cells co-expressing m-cherry2-PLIN2 and GFP-PLIN1ΔΔ were treated with 250 μM Na^+ oleate for 6 h.

(K) Deletion of the iMS and pMS switches PLIN1 from an integral to a class II LD protein. Domain colors as in (A).

See also Figure S3.

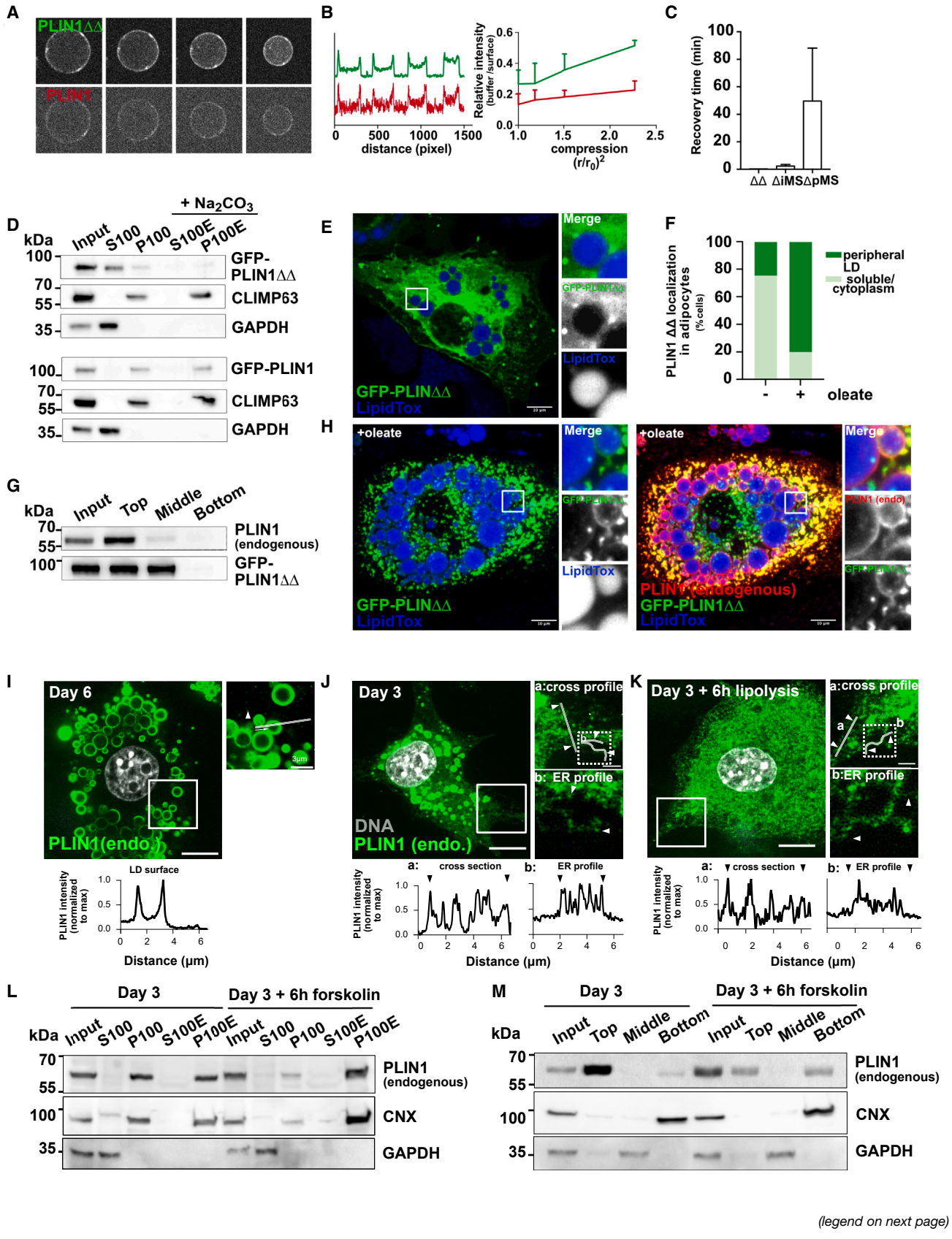

(legend on next page)

Perturbation of PLIN1 membrane targeting leads to an LD class switch in adipocytes

To test these interpretations directly in adipocytes, we stably integrated GFP-PLIN1 and GFP-PLIN1ΔΔ as inducible transgenes into 3T3L1 preadipocytes. Consistent with the results above, PLIN1ΔΔ was soluble (Figure 4D), and full-length PLIN1 behaved like an integral membrane protein (Figures 4D and 4E). PLIN1 localized to LDs after FA feeding, and, as in COS7 cells, moved from the ER to LDs even when translation was shut off with cycloheximide before LD induction (Figures S4B–S4E).

After expression of the transgene in day 6 adipocytes, PLIN1ΔΔ behaved like a class II LD protein, being largely excluded from the big LDs, which formed during differentiation (Figures 4E and 4F). Endogenous full-length PLIN1 was expressed and floated with the LDs to the top fraction (Figure 4G). PLIN1ΔΔ was additionally found in the soluble middle fraction, confirming the microscopy experiments (Figures 4E and 4F). Although being effectively excluded from the LDs covered by endogenous PLIN1 in cells, PLIN1ΔΔ remains LD binding competent and partially floats (Figure 4G), likely getting access to TAGs when LDs break during mechanical cell lysis.

Importantly, PLIN1ΔΔ efficiently moved from the cytoplasm to the peripheral LD population, which forms after FA feeding (Figures 4H and 4F). Consistent with the results shown for PLIN2–PLIN4 in Figure 1, PLIN1ΔΔ remained largely excluded from the LDs that were covered by endogenously expressed full-length PLIN1 (Figures 4H and 4F).

Taken together, these data suggest that removing the iMS and pMS not only reduced LD affinity and turned PLIN1ΔΔ into a class II LD protein but also leads to a change in LD class specificity (Figure S4F).

Finally, we examined the localization of endogenously expressed PLIN1 during adipocyte differentiation. As expected, in day 6 adipocytes, PLIN1 localized almost exclusively to the surface of LDs (Figure 4I). However, at earlier time points (e.g., day 3), endogenous PLIN1 is also abundantly present on the peripheral ER (Figure 4J;[10,44,45]) as a completely alkali-resistant integral membrane protein (Figure 4L). At this stage of differentiation, PLIN1 is probably stockpiled in the ER, facilitating rapid expansion of the LD surface.

Interestingly, when we triggered, at these stages, the breakdown of the LDs by activating lipolysis, PLIN1 efficiently moved back to the ER (Figures 4K–4L). The movement between LDs and the ER was further supported by flotation experiments, showing that stimulation of lipolysis re-distributed PLIN1 away from the remaining floating LDs into the membrane pellet (Figure 4M).

DISCUSSION

Here, we have shown that, contrary to its previous classification, PLIN1 behaves as an integral membrane protein and is not classical class II LD protein. We reveal that an unconventional, monotopic iMS is necessary and sufficient for integration into the ER membrane and facilitates high-affinity binding to the LD.

PLIN1 moves onto the LDs as soon as they appear during adipocyte differentiation. Due to its high affinity, it excludes the other PLINs from these LDs already at the earliest stages of the biosynthesis process. Up until day 3 post differentiation, the ER and LD pools readily exchange. However, at later stages (starting from day 6), PLIN1 is kinetically "trapped" on the surface of the first LD class. As a result, the second LD class, which emerges upon FA feeding, gets covered by PLIN2–PLIN4, which are class II PLINs targeting the second LD population from the cytoplasm.

Although we show, with translation shut-off experiments, that PLIN1 moves from the ER to the LD surface, it remains to be determined whether PLIN1 uses the conventional ERTOLD pathway (Figure S4F, ER→LD). The length of the iMS of around 30 amino acids (Figure S4G) fits the size of known hairpin motifs, but the iMS exhibits surprisingly low hydrophobicity and does, therefore, not satisfy the basic definition of a conventional ER membrane anchor.[46–48] The iMS contains some features that are also found in other hairpins that move between the ER and the LDs,[13] such as prolines and large tryptophans at the center of the motif (Figure S4G). Additionally, the iMS is flanked by positively charged residues (Figure S4G),[13] perhaps ensuring the

Figure 4. Membrane insertion determines LD class specificity by tuning LD binding kinetics

(A) Localization of GFP-PLIN1ΔΔ and mCherry-PLIN1 in an buffer-in-oil system with shrinking aqueous phase progressively shrinks.

(B) Intensity ratio of signal at the oil-buffer interface and within buffer for the indicated compression ratios. GFP-PLIN1ΔΔ, green; mCherry-PLIN1, red. $n = 3$ independent experiments, mean ± SD.

(C) Fluorescence recovery after photobleaching with oleate-treated Huh7 cells expressing GFP-PLIN1ΔΔ, ΔiMS, or ΔpMS. Scale bar, 10 μm. $n = 3$ experiments; results are expressed as mean ± SD.

(D) GFP-PLIN1ΔΔ or GFP-PLIN1 were expressed in 3T3-L1 cells from inducible transgenes and subjected to fractionation and alkaline extraction. Labeling as in Figure 2. CLIMP-63, integral ER membrane protein.

(E) As in (D) but with adipocytes. PLIN1ΔΔ was induced 6 days post differentiation with 500 ng/mL anhydrotetracycline for 6 h. LDs were stained with LipidToxDeepRed. Scale bar, 10 μm.

(**F**) Percentage of cells in (E) and (H) with GFP-PLIN1ΔΔ on peripheral LDs or in the cytoplasm; $n = 100$ cells.

(G) As in (E) but with flotation. Endogenous PLIN1 and GFP-PLIN1ΔΔ were both detected with an anti-PLIN1 antibody.

(H) As in (E) but with oleate for 6 h. GFP-PLIN1ΔΔ is now found on peripheral LDs. PLIN1ΔΔ remains excluded from the LDs covered by endogenous PLIN1. On the right, an anti-PLIN1 antibody stains both endogenous PLIN1 on large LDs (red) and PLIN1ΔΔ on the peripheral LDs (GFP+red = yellow).

(I) Endogenous PLIN1 in day 6 adipocytes; shown is a line plot of PLIN1 intensity (normalized to maximum), as drawn in the inset. Scale bar: 10 μm; for inset, 4 μm.

(J) As in (I) but at day 3. Arrowheads mark terminal points of the ER profile.

(K) As in (J) but after addition of 10 μM forskolin for 6 h.

(L) Fractionation and alkaline extraction of adipocytes as in (J) and (K); labels as in (D).

(M) Flotation experiment of the cells as in (J) and (K), done as in (G).

See also Figure S4.

correct membrane topology or contributing to the regulation of LD access and stability on the LD surface.

Consistent with other work,[49] our data indicate that the iMS favors the LD surface over the ER bilayer, likely explaining why, in adipocytes, the steady-state ER pool is minimal. Since PLIN1 targets LDs early during biogenesis, it probably enters the LD through the Seipin complex.[28,50] Movement to the LD may later on switch to the bridge pathway that was recently identified[51] in the fly, which bears molecular similarity to ER-LD contact site machinery previously identified in 3T3-L1 cells.[52] Our alkaline extraction data and detailed structure-function analysis seem to be incompatible with a cytoplasmic targeting pathway (Figure S4F, ER→cytoplasm→LD) but do not fully exclude this possibility.

The PLIN1-covered LDs are essential for adipose tissue function; loss of PLIN1 in mice and humans can cause lipodystrophy[4,53] because increased basal adipose lipolysis prevents efficient LD expansion.[54,55] The affected patients are highly insulin resistant and suffer from hypertriglyceridemia, cardiovascular defects, and fatty liver disease.[55,56] Partial loss of PLIN1 or PLIN1 haploinsufficiency can, surprisingly, have beneficial effects on metabolic health.[57] According to recent reports, some PLIN1 mutants in fact improve metabolic profiles and reduce risk for cardiovascular disease.[58,59] Controlled perturbation of PLIN1 membrane targeting might therefore open avenues for mechanism-based therapy of fatty liver disease, type 2 diabetes, and obesity.

Limitations of this study

A limitation of our study is that adipocyte differentiation in tissue culture may not fully recapitulate the process in real tissue. Future work will address the physiological function of the two LD classes that form in tissue culture.

Another open question is how PLIN1 is targeted to the ER. The simplest model involves membrane integration by Sec61.[60] However, since the hydrophobicity of the iMS is relatively low, the pathway may depend on the ER membrane complex or requires a chaperone, such as GET3/TRC40.[61] It is further still a possibility that, in adipocytes, PLIN1 is first inserted into the LD surface and then moves to the ER. However, if this were true, then the acutely forming smaller LDs would be covered by PLIN1 and not by different PLIN family members.

Lastly, it is likely that additional machinery is required to form the two LD populations. We currently speculate that PLIN1 transport to the LDs is gated. The involved machinery may depend on the Seipin complex, which probably contributes to the enrichment of PLIN1 on the surface of the first LD class and restricts the movement back to the ER in later stages of differentiation. Gated exchange between the ER and the PLIN1 LD surface likely contributes to the formation of LD heterogeneity.

STAR★METHODS

Detailed methods are provided in the online version of this paper and include the following:

SUPPLEMENTAL INFORMATION

Supplemental information can be found online at https://doi.org/10.1016/j.celrep.2024.114093.

ACKNOWLEDGMENTS

We thank Pedro Carvalho (University of Oxford) for critical reading of the manuscript and Lucas Pelkmans (University of Zurich) for generous support with research infrastructure. A.R.T. was supported by ANR-MOBIL and ANR-21-CE11-LIPRODYN. R.W.K. acknowledges support from the SNSF (SNF 31003A_159793), the Helmut Horten Foundation, the E.P. Abraham Cephalosporin Fund, the John Fell Oxford University Press Research Fund, and a grant from Diabetes UK (22/0006453).

AUTHOR CONTRIBUTIONS

Conceptualization, R.W.K.; methodology, M.M., R.W.K., and A.R.T.; formal analysis, M.M., O.S., D.A., K.B.M., M.O., A.R.T., and R.W.K.; investigation, M.M., O.S., D.A., K.B., M.O., A.R.T., and R.W.K.; resources, A.R.T. and R.W.K.; writing – original draft, R.W.K.; writing – review & editing, M.M., O.S., A.R.T., and R.W.K., visualization, M.M., O.S., A.R.T., and R.W.K.; supervision, A.R.T. and R.W.K.; funding acquisition; A.R.T. and R.W.K.

DECLARATION OF INTERESTS

The authors declare no competing interests.

Received: November 3, 2021
Revised: March 12, 2024
Accepted: March 27, 2024
Published: April 10, 2024

REFERENCES

1. Rosen, E.D., and Spiegelman, B.M. (2006). Adipocytes as regulators of energy balance and glucose homeostasis. Nature *444*, 847–853. https://doi.org/10.1038/nature05483.
2. Morigny, P., Boucher, J., Arner, P., and Langin, D. (2021). Lipid and glucose metabolism in white adipocytes: pathways, dysfunction and therapeutics. Nat. Rev. Endocrinol. *17*, 276–295. https://doi.org/10.1038/s41574-021-00471-8.
3. Grabner, G.F., Xie, H., Schweiger, M., and Zechner, R. (2021). Lipolysis: cellular mechanisms for lipid mobilization from fat stores. Nat. Metab. *3*, 1445–1465. https://doi.org/10.1038/s42255-021-00493-6.
4. Robbins, A.L., and Savage, D.B. (2015). The genetics of lipid storage and human lipodystrophies. Trends Mol. Med. *21*, 433–438. https://doi.org/10.1016/j.molmed.2015.04.004.
5. Samuel, V.T., and Shulman, G.I. (2012). Mechanisms for Insulin Resistance: Common Threads and Missing Links. Cell *148*, 852–871. https://doi.org/10.1016/j.cell.2012.02.017.
6. Guilherme, A., Virbasius, J.V., Puri, V., and Czech, M.P. (2008). Adipocyte dysfunctions linking obesity to insulin resistance and type 2 diabetes. Nat. Rev. Mol. Cell Biol. *9*, 367–377. https://doi.org/10.1038/nrm2391.
7. Olzmann, J.A., and Carvalho, P. (2019). Dynamics and functions of lipid droplets. Nat. Rev. Mol. Cell Biol. *20*, 137–155. https://doi.org/10.1038/s41580-018-0085-z.
8. Walther, T.C., Chung, J., and Farese, R.V. (2017). Lipid Droplet Biogenesis. Annu. Rev. Cell Dev. Biol. *33*, 491–510. https://doi.org/10.1146/annurev-cellbio-100616-060608.
9. Pol, A., Gross, S.P., and Parton, R.G. (2014). Review: biogenesis of the multifunctional lipid droplet: lipids, proteins, and sites. J. Cell Biol. *204*, 635–646. https://doi.org/10.1083/jcb.201311051.
10. Wolins, N.E., Quaynor, B.K., Skinner, J.R., Schoenfish, M.J., Tzekov, A., and Bickel, P.E. (2005). S3-12, Adipophilin, and TIP47 package lipid in adipocytes. J. Biol. Chem. *280*, 19146–19155. https://doi.org/10.1074/jbc.m500978200.
11. Wolins, N.E., Quaynor, B.K., Skinner, J.R., Tzekov, A., Croce, M.A., Gropler, M.C., Varma, V., Yao-Borengasser, A., Rasouli, N., Kern, P.A., et al. (2006). OXPAT/PAT-1 is a PPAR-induced lipid droplet protein that promotes fatty acid utilization. Diabetes *55*, 3418–3428. https://doi.org/10.2337/db06-0399.
12. Kassan, A., Herms, A., Fernández-Vidal, A., Bosch, M., Schieber, N.L., Reddy, B.J.N., Fajardo, A., Gelabert-Baldrich, M., Tebar, F., Enrich, C., et al. (2013). Acyl-CoA synthetase 3 promotes lipid droplet biogenesis in ER microdomains. J. Cell Biol. *203*, 985–1001. https://doi.org/10.1083/jcb.201305142.
13. Olarte, M.-J., Kim, S., Sharp, M.E., Swanson, J.M.J., Farese, R.V., and Walther, T.C. (2020). Determinants of Endoplasmic Reticulum-to-Lipid Droplet Protein Targeting. Dev. Cell *54*, 471–487.e7. https://doi.org/10.1016/j.devcel.2020.07.001.
14. Dhiman, R., Caesar, S., Thiam, A.R., and Schrul, B. (2020). Mechanisms of protein targeting to lipid droplets: A unified cell biological and biophysical perspective. Semin. Cell Dev. Biol. *108*, 4–13. https://doi.org/10.1016/j.semcdb.2020.03.004.
15. Mathiowetz, A.J., and Olzmann, J.A. (2024). Lipid droplets and cellular lipid flux. Nat. Cell Biol. *26*, 331–345. https://doi.org/10.1038/s41556-024-01364-4.
16. Wilfling, F., Wang, H., Haas, J.T., Krahmer, N., Gould, T.J., Uchida, A., Cheng, J.-X., Graham, M., Christiano, R., Fröhlich, F., et al. (2013). Triacylglycerol synthesis enzymes mediate lipid droplet growth by relocalizing from the ER to lipid droplets. Dev. Cell *24*, 384–399. https://doi.org/10.1016/j.devcel.2013.01.013.
17. Eisenberg-Bord, M., Mari, M., Weill, U., Rosenfeld-Gur, E., Moldavski, O., Castro, I.G., Soni, K.G., Harpaz, N., Levine, T.P., Futerman, A.H., et al. (2018). Identification of seipin-linked factors that act as determinants of a lipid droplet subpopulation. J. Cell Biol. *217*, 269–282. https://doi.org/10.1083/jcb.201704122.
18. Chitraju, C., Mejhert, N., Haas, J.T., Diaz-Ramirez, L.G., Grueter, C.A., Imbriglio, J.E., Pinto, S., Koliwad, S.K., Walther, T.C., and Farese, R.V., Jr. (2017). Triglyceride Synthesis by DGAT1 Protects Adipocytes from Lipid-Induced ER Stress during Lipolysis. Cell Metab. *26*, 407–418.e3. https://doi.org/10.1016/j.cmet.2017.07.012.
19. Thiam, A.R., and Beller, M. (2017). The why, when and how of lipid droplet diversity. J. Cell Sci. *130*, 315–324. https://doi.org/10.1242/jcs.192021.
20. Straub, B.K., Stoeffel, P., Heid, H., Zimbelmann, R., and Schirmacher, P. (2008). Differential pattern of lipid droplet-associated proteins and de novo perilipin expression in hepatocyte steatogenesis. Hepatology *47*, 1936–1946. https://doi.org/10.1002/hep.22268.
21. Hsieh, K., Lee, Y.K., Londos, C., Raaka, B.M., Dalen, K.T., and Kimmel, A.R. (2012). Perilipin family members preferentially sequester to either triacylglycerol-specific or cholesteryl-ester-specific intracellular lipid storage droplets. J. Cell Sci. *125*, 4067–4076. https://doi.org/10.1242/jcs.104943.
22. Herms, A., Bosch, M., Ariotti, N., Reddy, B.J.N., Fajardo, A., Fernández-Vidal, A., Alvarez-Guaita, A., Fernández-Rojo, M.A., Rentero, C., Tebar, F., et al. (2013). Cell-to-cell heterogeneity in lipid droplets suggests a mechanism to reduce lipotoxicity. Curr. Biol. *23*, 1489–1496. https://doi.org/10.1016/j.cub.2013.06.032.
23. Henne, M., Goodman, J.M., and Hariri, H. (2020). Spatial compartmentalization of lipid droplet biogenesis. Biochim. Biophys. Acta. Mol. Cell Biol. Lipids *1865*, 158499. https://doi.org/10.1016/j.bbalip.2019.07.008.
24. Ugrankar, R., Bowerman, J., Hariri, H., Chandra, M., Chen, K., Bossanyi, M.-F., Datta, S., Rogers, S., Eckert, K.M., Vale, G., et al. (2019). Drosophila Snazarus Regulates a Lipid Droplet Population at Plasma Membrane-Droplet Contacts in Adipocytes. Dev. Cell *50*, 557–572.e5. https://doi.org/10.1016/j.devcel.2019.07.021.
25. Heid, H., Rickelt, S., Zimbelmann, R., Winter, S., Schumacher, H., Dörflinger, Y., Kuhn, C., and Franke, W.W. (2014). On the formation of lipid droplets in human adipocytes: the organization of the perilipin-vimentin cortex. PLoS One *9*, e90386. https://doi.org/10.1371/journal.pone.0090386.
26. Wolins, N.E., Brasaemle, D.L., and Bickel, P.E. (2006). A proposed model of fat packaging by exchangeable lipid droplet proteins. FEBS Lett. *580*, 5484–5491. https://doi.org/10.1016/j.febslet.2006.08.040.
27. Freyre, C.A.C., Rauher, P.C., Ejsing, C.S., and Klemm, R.W. (2019). MIGA2 Links Mitochondria, the ER, and Lipid Droplets and Promotes De Novo Lipogenesis in Adipocytes. Mol. Cell *76*, 811–825.e14. https://doi.org/10.1016/j.molcel.2019.09.011.
28. Kory, N., Farese, R.V., and Walther, T.C. (2016). Targeting Fat: Mechanisms of Protein Localization to Lipid Droplets. Trends Cell Biol. *26*, 535–546. https://doi.org/10.1016/j.tcb.2016.02.007.
29. Olarte, M.-J., Swanson, J.M.J., Walther, T.C., and Farese, R.V. (2022). The CYTOLD and ERTOLD pathways for lipid droplet–protein targeting. Trends Biochem. Sci. *47*, 39–51. https://doi.org/10.1016/j.tibs.2021.08.007.
30. Prévost, C., Sharp, M.E., Kory, N., Lin, Q., Voth, G.A., Farese, R.V., and Walther, T.C. (2018). Mechanism and Determinants of Amphipathic Helix-Containing Protein Targeting to Lipid Droplets. Dev. Cell *44*, 73–86.e4. https://doi.org/10.1016/j.devcel.2017.12.011.
31. Kory, N., Thiam, A.-R., Farese, R.V., and Walther, T.C. (2015). Protein Crowding Is a Determinant of Lipid Droplet Protein Composition. Dev. Cell *34*, 351–363. https://doi.org/10.1016/j.devcel.2015.06.007.
32. Rowe, E.R., Mimmack, M.L., Barbosa, A.D., Haider, A., Isaac, I., Ouberai, M.M., Thiam, A.R., Patel, S., Saudek, V., Siniossoglou, S., and Savage, D.B. (2016). Conserved Amphipathic Helices Mediate Lipid Droplet

Targeting of Perilipins 1-3. J. Biol. Chem. *291*, 6664–6678. https://doi.org/10.1074/jbc.m115.691048.

33. Čopič, A., Antoine-Bally, S., Giménez-Andrés, M., La Torre Garay, C., Antonny, B., Manni, M.M., Pagnotta, S., Guihot, J., and Jackson, C.L. (2018). A giant amphipathic helix from a perilipin that is adapted for coating lipid droplets. Nat. Commun. *9*, 1332. https://doi.org/10.1038/s41467-018-03717-8.
34. Giménez-Andrés, M., Emeršič, T., Antoine-Bally, S., D'Ambrosio, J.M., Antonny, B., Derganc, J., and Čopič, A. (2021). Exceptional stability of a perilipin on lipid droplets depends on its polar residues, suggesting multimeric assembly. Elife *10*, e61401. https://doi.org/10.7554/elife.61401.
35. Chorlay, A., Monticelli, L., Veríssimo Ferreira, J., M'barek, K.B., Ajjaji, D., Wang, S., Johnson, E., Beck, R., Omrane, M., Beller, M., et al. (2019). Membrane Asymmetry Imposes Directionality on Lipid Droplet Emergence from the ER. Dev. Cell *50*, 25–42.e7. https://doi.org/10.1016/j.devcel.2019.05.003.
36. Bickel, P.E., Tansey, J.T., and Welte, M.A. (2009). PAT proteins, an ancient family of lipid droplet proteins that regulate cellular lipid stores. Biochim. Biophys. Acta *1791*, 419–440. https://doi.org/10.1016/j.bbalip.2009.04.002.
37. Londos, C., Brasaemle, D.L., Schultz, C.J., Segrest, J.P., and Kimmel, A.R. (1999). Perilipins, ADRP, and other proteins that associate with intracellular neutral lipid droplets in animal cells. Semin. Cell Dev. Biol. *10*, 51–58. https://doi.org/10.1006/scdb.1998.0275.
38. Kimmel, A.R., and Sztalryd, C. (2016). The Perilipins: Major Cytosolic Lipid Droplet–Associated Proteins and Their Roles in Cellular Lipid Storage, Mobilization, and Systemic Homeostasis. Annu. Rev. Nutr. *36*, 471–509. https://doi.org/10.1146/annurev-nutr-071813-105410.
39. Brasaemle, D.L. (2007). Thematic review series: adipocyte biology. The perilipin family of structural lipid droplet proteins: stabilization of lipid droplets and control of lipolysis. J. Lipid Res. *48*, 2547–2559. https://doi.org/10.1194/jlr.r700014-jlr200.
40. Garcia, A., Subramanian, V., Sekowski, A., Bhattacharyya, S., Love, M.W., and Brasaemle, D.L. (2004). The amino and carboxyl termini of perilipin a facilitate the storage of triacylglycerols. J. Biol. Chem. *279*, 8409–8416. https://doi.org/10.1074/jbc.m311198200.
41. Choi, Y.M., Ajjaji, D., Fleming, K.D., Borbat, P.P., Jenkins, M.L., Moeller, B.E., Fernando, S., Bhatia, S.R., Freed, J.H., Burke, J.E., et al. (2023). Structural insights into perilipin 3 membrane association in response to diacylglycerol accumulation. Nat. Commun. *14*, 3204. https://doi.org/10.1038/s41467-023-38725-w.
42. Garcia, A., Sekowski, A., Subramanian, V., and Brasaemle, D.L. (2003). The central domain is required to target and anchor perilipin A to lipid droplets. J. Biol. Chem. *278*, 625–635. https://doi.org/10.1074/jbc.m206602200.
43. Ajjaji, D., M'barek, K.B., Mimmack, M.L., England, C., Herscovitz, H., Dong, L., Kay, R.G., Patel, S., Saudek, V., Small, D.M., et al. (2019). Dual binding motifs underpin the hierarchical association of perilipins1–3 with lipid droplets. Mol. Biol. Cell *30*, 703–716. https://doi.org/10.1091/mbc.e18-08-0534.
44. Wolins, N.E., Skinner, J.R., Schoenfish, M.J., Tzekov, A., Bensch, K.G., and Bickel, P.E. (2003). Adipocyte protein S3-12 coats nascent lipid droplets. J. Biol. Chem. *278*, 37713–37721. https://doi.org/10.1074/jbc.m304025200.
45. Skinner, J.R., Harris, L.-A.L.S., Shew, T.M., Abumrad, N.A., and Wolins, N.E. (2013). Perilipin 1 moves between the fat droplet and the endoplasmic reticulum. Adipocyte *2*, 80–86. https://doi.org/10.4161/adip.22864.
46. Shibata, Y., Hu, J., Kozlov, M.M., and Rapoport, T.A. (2009). Mechanisms shaping the membranes of cellular organelles. Annu. Rev. Cell Dev. Biol. *25*, 329–354. https://doi.org/10.1146/annurev.cellbio.042308.113324.
47. Parton, R.G., and del Pozo, M.A. (2013). Caveolae as plasma membrane sensors, protectors and organizers. Nat. Rev. Mol. Cell Biol. *14*, 98–112. https://doi.org/10.1038/nrm3512.
48. Schrul, B., and Kopito, R.R. (2016). Peroxin-dependent targeting of a lipid-droplet-destined membrane protein to ER subdomains. Nat. Cell Biol. *18*, 740–751. https://doi.org/10.1038/ncb3373.
49. Caillon, L., Nieto, V., Gehan, P., Omrane, M., Rodriguez, N., Monticelli, L., and Thiam, A.R. (2020). Triacylglycerols sequester monotopic membrane proteins to lipid droplets. Nat. Commun. *11*, 3944. https://doi.org/10.1038/s41467-020-17585-8.
50. Wilfling, F., Thiam, A.R., Olarte, M.-J., Wang, J., Beck, R., Gould, T.J., Allgeyer, E.S., Pincet, F., Bewersdorf, J., Farese, R.V., and Walther, T.C. (2014). Arf1/COPI machinery acts directly on lipid droplets and enables their connection to the ER for protein targeting. Elife *3*, e01607. https://doi.org/10.7554/elife.01607.
51. Song, J., Mizrak, A., Lee, C.-W., Cicconet, M., Lai, Z.W., Tang, W.-C., Lu, C.-H., Mohr, S.E., Farese, R.V., and Walther, T.C. (2022). Identification of two pathways mediating protein targeting from ER to lipid droplets. Nat. Cell Biol. *24*, 1364–1377. https://doi.org/10.1038/s41556-022-00974-0.
52. Xu, D., Li, Y., Wu, L., Li, Y., Zhao, D., Yu, J., Huang, T., Ferguson, C., Parton, R.G., Yang, H., and Li, P. (2018). Rab18 promotes lipid droplet (LD) growth by tethering the ER to LDs through SNARE and NRZ interactions. J. Cell Biol. *217*, 975–995. https://doi.org/10.1083/jcb.201704184.
53. Mann, J.P., and Savage, D.B. (2019). What lipodystrophies teach us about the metabolic syndrome. J. Clin. Invest. *129*, 4009–4021. https://doi.org/10.1172/jci129190.
54. Tansey, J.T., Sztalryd, C., Gruia-Gray, J., Roush, D.L., Zee, J.V., Gavrilova, O., Reitman, M.L., Deng, C.-X., Li, C., Kimmel, A.R., and Londos, C. (2001). Perilipin ablation results in a lean mouse with aberrant adipocyte lipolysis, enhanced leptin production, and resistance to diet-induced obesity. Proc. Natl. Acad. Sci. USA *98*, 6494–6499. https://doi.org/10.1073/pnas.101042998.
55. Gandotra, S., Lim, K., Girousse, A., Saudek, V., O'Rahilly, S., and Savage, D.B. (2011). Human frame shift mutations affecting the carboxyl terminus of perilipin increase lipolysis by failing to sequester the adipose triglyceride lipase (ATGL) coactivator AB-hydrolase-containing 5 (ABHD5). J. Biol. Chem. *286*, 34998–35006. https://doi.org/10.1074/jbc.m111.278853.
56. Garg, A. (2011). Clinical review#: Lipodystrophies: genetic and acquired body fat disorders. J. Clin. Endocrinol. Metab. *96*, 3313–3325. https://doi.org/10.1210/jc.2011-1159.
57. Melvin, A., Stears, A., and Savage, D.B. (2019). Recent developments in lipodystrophy. Curr. Opin. Lipidol. *30*, 284–290. https://doi.org/10.1097/mol.0000000000000613.
58. Koprulu, M., Zhao, Y., Wheeler, E., Dong, L., Rocha, N., Li, C., Griffin, J.D., Patel, S., Van de Streek, M., Glastonbury, C.A., et al. (2022). Identification of rare loss of function genetic variation regulating body fat distribution. J. Clin. Endocrinol. Metab. *107*, 1065–1077. https://doi.org/10.1210/clinem/dgab877.
59. Patel, K.A., Burman, S., Laver, T.W., Hattersley, A.T., Frayling, T.M., and Weedon, M.N. (2022). PLIN1 Haploinsufficiency Causes a Favorable Metabolic Profile. J. Clin. Endocrinol. Metab. *107*, e2318–e2323. https://doi.org/10.1210/clinem/dgac104.
60. Rapoport, T.A., Li, L., and Park, E. (2017). Structural and Mechanistic Insights into Protein Translocation. Annu. Rev. Cell Dev. Biol. *33*, 369–390. https://doi.org/10.1146/annurev-cellbio-100616-060439.
61. Hegde, R.S., and Keenan, R.J. (2022). The mechanisms of integral membrane protein biogenesis. Nat. Rev. Mol. Cell Biol. *23*, 107–124. https://doi.org/10.1038/s41580-021-00413-2.
62. Battich, N., Stoeger, T., and Pelkmans, L. (2015). Control of Transcript Variability in Single Mammalian Cells. Cell *163*, 1596–1610. https://doi.org/10.1016/j.cell.2015.11.018.
63. Snijder, B., Sacher, R., Ramo, P., Damm, E.M., Liberali, P., and Pelkmans, L. (2009). Population context determines cell-to-cell variability in endocytosis and virus infection. Nature *461*, 520–523. https://doi.org/10.1038/nature08282.

STAR★METHODS

KEY RESOURCES TABLE

REAGENT or RESOURCE	SOURCE	IDENTIFIER
Antibodies		
Mouse monoclonal c-Myc, 1:200	Santa Cruz	Cat#: sc-40
Rabbit polyclonal Calreticulin, 1:1000	Abcam	Cat#: ab2907; RRID:AB_303402
Mouse monoclonal FLAG, 1:200	Sigma-Aldrich	Cat#: F3165; RRID:AB_259529
Mouse monoclonal HA, 1:200	Roche	Cat#: 11583816001; RRID:AB_514505
Goat polyclonal PLIN1, 1:200	Abcam	Cat#: ab61682; RRID:AB_944751
Rabbit monoclonal PLIN1 , 1:200 (Figures 4I–4M)	Cell Signaling	Cat#: #9349; RRID:AB_10829911
Rabbit polyclonal PLIN2, 1:200	Abcam	Cat#: ab52355; RRID:AB_867527
Rabbit polyclonal PLIN3, 1:200	Millipore	Cat#: ABS482
Rabbit polyclonal PLIN4, 1:200	Sigma-Aldrich	Cat#: ABS526
Rabbit polyclonal Calnexin (CNX), 1:200	Proteintech	Cat#: 10427-2-AP; RRID:AB_2069033
Rabbit polyclonal CKAP4 (CLIMP63), 1:200	Bethyl Laboratories	Cat#: A302-257A; RRID:AB_1731083
Donkey anti-goat IgG Alexa Fluor 488, 1:500	Thermo-Fisher	Cat#: A11055; RRID:AB_2534102
Donkey anti-goat IgG Alexa Fluor 568, 1:500	Thermo-Fisher	Cat#: A11057; RRID:AB_2534104
Donkey anti-goat IgG Alexa Fluor 647, 1:500	Thermo-Fisher	Cat#: A21447; RRID:AB_2535864
Donkey anti-mouse IgG Alexa Fluor 488, 1:500	Thermo-Fisher	Cat#: A21202: RRID:AB_141607
Donkey anti-mouse IgG Alexa Fluor 568, 1:500	Thermo-Fisher	Cat#: A10042; RRID:AB_2534017
Donkey anti-mouse IgG Alexa Fluor 647, 1:500	Thermo-Fisher	Cat#: A31571; RRID:AB_162542
Donkey anti-rabbit IgG Alexa Fluor 488, 1:500	Thermo-Fisher	Cat#: A21206; RRID:AB_2535792
Donkey anti-rabbit IgG Alexa Fluor 568, 1:500	Thermo-Fisher	Cat#: A10042; RRID:AB_2534017
Donkey anti-rabbit IgG Alexa Fluor 647, 1:500	Thermo-Fisher	Cat#: A31573; RRID:AB_2536183
Donkey anti-goat HRP, 1:2500	Bethyl	Cat#: A50-201P; RRID:AB_66756
Donkey anti-mouse HRP, 1:5000	Promega	Cat#: W4021; RRID:AB_430834
Donkey anti-rabbit HRP, 1:5000	Promega	Cat#: W4011; RRID:AB_430833
Chemicals, peptides, and recombinant proteins		
DMEM	GIBCO	Cat#41965-039
Fetal bovine serum	Sigma-Aldrich	Cat#F7524
Calf serum	Sigma-Aldrich	Cat#12133C
OptiMEM	GIBCO	Cat#11058-021
Non-essential amino acids	Sigma	Cat#M7145
Sodium Pyruvate	GIBCO	Cat#11360 070; CAS: 113-24-6
Puromycin	Invivogen	Cat#ant-pr-1; CAS: 58-58-2
Geneticin G418	Invivogen	Cat#ant-gn-1; CAS: 108321-42-2
Paraformaldehyde	Electron Microscopy Sciences	Cat#15711; CAS: 50-00-0
Triton X-100	Thermo Fisher Scientific	Cat#28314; CAS: 9002-93-1
Hexadimethrine bromide (polybrene)	Sigma-Aldrich	Cat#107689; CAS: 28728-55-4
Oleic Acid	Sigma-Aldrich	Cat#O1383-5G; CAS: 112-80-1
HCS LipidTOX Red Neutral Lipid Stain	Thermo-Fisher	Cat#H34476
HCS LipidTOX Deep Red Neutral Lipid Stain	Thermo Fisher Scientific	Cat#H34477
Fluoromount-G	SouthernBiotech	Cat#0100-01; CAS: 0100-01
Dexamethasone	G-Biosciences	Cat#API-04; CAS: 50-02-2
3-Isobutyl-1-methylxanthine	Sigma-Aldrich	Cat#I5879; CAS: 28822-58-4
Insulin	Sigma-Aldrich	Cat#I0516-5ML; CAS: 11070-73-8
Cycloheximide	Sigma-Aldrich	Cat#C7698; CAS: 66-81-9

(*Continued on next page*)

Continued

REAGENT or RESOURCE	SOURCE	IDENTIFIER
Forskolin	Sigma-Aldrich	Cat#F3917-10MG; CAS: 66575-29-9
Atto490LS NHS Ester	Atto-tec	Cat#AD 490LS-31
Alexa Fluor 647 NHS Ester	Life Technologies	Cat#SE-af647
cOmplete, Mini Protease Inhibitor Cocktail	Sigma Aldrich	Cat#11836153001
Ionic Detergent Compatibility Reagent for Pierce	Thermo Fisher Scientific	Cat#22663
D-Glucose [U-14C]	Hartmann analytic	Cat#MC 144W
Doxycycline hyclate	Sigma-Aldrich	Cat#D9891-1G; CAS: 24390-14-5
Chloroform	Rathburn Chemicals	Cat#RH1009; CAS: 67-66-3
Methanol	Biosolve Chemicals	Cat#13687802; CAS: 67-56-1
Propanol	Sigma-Aldrich	Cat#650447; CAS: 67-63-0
Critical commercial assays		
Pierce 660 nm Protein Assay Reagent	Thermo Fisher Scientific	Cat#22660
Experimental models: Cell lines		
Mouse 3T3-L1 cells	ATCC	Cat#CL-173; RRID: CVCL_0123
Monkey COS-7 cells	Tom A. Rapoport, Harvard Medical School, Boston, USA	RRID: CVCL_0224
Human HEK293T cells	Dharmacon	Cat#TLP5918; RRID: CVCL_0063
Oligonucleotides		
Oligonucleotides for recombinant DNA (see below)	This study	Table S1
Recombinant DNA		
mEGFP-N1	Michael Davidson Lab	Addgene 54767
mEGFP-C1	Michael Davidson Lab	Addgene 54759
mCherry2-C1	Michael Davidson Lab	Addgene 54563
mCherry2-N1	Michael Davidson Lab	Addgene 54517
pINDUCER20	Stephen Elledge Lab	Addgene 44012
pINDUCER21	Stephen Elledge & Thomas Westbrook Lab	Addgene 46948
psPAX2	Didier Trono Lab	Addgene 12260
pMD2.G	Didier Trono Lab	Addgene 12259
GFP-PLIN1	This study	N/A
GFP-PLIN2	This study	N/A
GFP-PLIN3	This study	N/A
GFP-PLIN1 1–192, 1–237, 1–281, 1-371	This study	N/A
GFP-PLIN1 192–517, 237–517, 281–517, 328–517, 347–517, 371-517	This study	N/A
GFP-PLIN1-ΔΔ (Δ238-280 Δ348-370)	This study	N/A
GFP-PLIN2+251InsiMS	This study	N/A
cDNA Mouse PLIN1	Dharmacon	MMM1013-202799812
cDNA Mouse PLIN3	Dharmacon	MMM1013-202764453
cDNA Mouse PLIN4	This study	Genscript custom synthesis
Software and algorithms		
MATLAB		https://www.mathworks.com/products/matlab.html
CellProfiler		https://github.com/pelkmanslab/CellProfilerPelkmans
CellProfiler Pelkmans Lab	Battich et al.[62]	https://github.com/pelkmanslab/CellProfilerPelkmans/tree/master/Modules
ImageJ	National Institutes of Health, USA	https://imagej.net/Welcome RRID: SCR_003070

(*Continued on next page*)

Continued

REAGENT or RESOURCE	SOURCE	IDENTIFIER
Other		
Round microscope cover glasses, 18 mm, No. 1	VWR	Cat#631–1580
Nikon Eclipse Ti E with CSU-W1 spinning disk	Nikon	N/A
Yokogawa CellVoyager 7000 with CSU-X1 spinning disk	Yokugawa	N/A
Leica SP5 confocal laser scanning microscope	Leica	N/A
Olympus SoRa spinning disc confocal microscope	Olympus	N/A

RESOURCE AVAILABILITY

Lead contact

Further information and requests for resources and reagents should be directed to and will be fulfilled by the lead contact, Robin Klemm (Robin.Klemm@dpag.ox.ac.uk).

Materials availability

All unique/stable reagents generated in this study are available from the lead contact with a completed materials transfer agreement.

Data and code availability

- Original/source data (images, gels, quantifications) reported in this paper will be shared by the lead contact upon request.
- This paper does not report original code.
- Any additional information required to reanalyze the data reported in this paper is available from the lead contact upon request.

EXPERIMENTAL MODEL AND STUDY PARTICIPANT DETAILS

Cell lines

COS-7 cells were a kind gift from Tom A. Rapoport (Harvard Medical School, Boston, USA). COS7 is a male African green monkey kidney fibroblast cell line. HEK293T cells were obtained from Dharmacon (#TLP5918). HEK293T is a female human embryonic kidney cell line. 3T3-L1 pre-adipocytes were from ATCC (CL-173). 3T3-L1 is a continuous sub-strain of male murine 3T3 (Swiss albino) cells, developed through clonal isolation.

Cell culture

COS-7 cells were maintained in Dulbeccos's Modified Eagle Medium with 4.5 g/L glucose and L-glutamine (DMEM, Thermo Fischer Scientific, #41965062), supplemented with 10% fetal bovine serum (FBS; Sigma-Aldrich, #F7524). HEK293T cells were maintained in DMEM containing 10% FBS, 25 mM HEPES (Sigma-Aldrich, H4034), 1 mM sodium pyruvate (Thermo-Fisher), 2 mM glutamine (Sigma-Aldrich) and 100 μM non-essential amino acids (Thermo-Fisher). All cells were kept as sub-confluent cultures and were sub-cultured regularly. All cell lines were periodically tested for mycoplasma and grown according to ATCC guidelines. Cells were incubated at 37°C and 5% CO_2.

METHOD DETAILS

Pre-adipocyte maintenance

3T3-L1 pre-adipocytes were obtained from ATCC (CL-173) and cultured in DMEM with 4.5 g/L glucose and L-glutamine (Thermo Fischer Scientific, #41965062), containing 10% calf serum (CS; Sigma-Aldrich, #12133C). Cells were grown as sub-confluent cultures in 10 cm tissue culture dishes (TPP) and sub-cultured regularly.

Adipocyte differentiation procedure

For the differentiation of 3T3-L1 pre-adipocytes into white adipocytes, the cells were first grown to confluence and kept as a confluent culture for 48 h. For differentiation in 96-well format, cells were seeded at a density of 10,000 cells per well of a 96-well plate (Greiner). Typically, the cells reached confluence the next day. After 48 hours of confluence differentiation was induced by the addition of adipocyte differentiation medium consisting of DMEM supplemented with 10% FBS, 172 nM bovine insulin (Sigma-Aldrich, #I0516), 500 μM 3-Isobutyl-1-methylxanthine (IBMX, Sigma-Aldrich #I5879), and 1 μM dexamethasone (Gbiosciences, #API-04). Cells were kept in differentiation medium for 48 hours. The differentiation medium was then replaced by DMEM containing 10% FBS and 172 nM bovine insulin. Cells were kept in the insulin medium for another 48 hours. At day four after induction of differentiation the insulin medium was replaced by DMEM containing 10% FBS. The medium was then refreshed every two days. Typically, cells were used for experiments at day 6 or day 8 after start of differentiation.

Transfection and subcellular fractionation and alkaline extraction

1.1 × 106 COS-7 cells were seeded on a 10 cm dish the one day before transfection. The next morning cells were transfected with 10 μg of the plasmid of interest using GeneJuice transfection reagent (Merck, #70967-3) according to the manufacturer's instructions. After 6 h of incubation at 37°C the medium was replaced with fresh DMEM containing 10% FBS. The cells were then incubated at 37°C/5% CO_2 overnight. The next morning the cells were washed once with ice-cold PBS and then harvested in 1 mL PBS with a cell scraper. The cells were briefly pelleted at 2000 g for 5 min at 4°C, and the supernatant was discarded. The cells were resuspended in 1 mL PBS containing protease inhibitor cocktail (cOmplete, Mini, EDTA-free Protease Inhibitor Cocktail; Merck, #11836153001) (PBSI) and lysed by 20 passages through a bead-homogenizer (Isobiotec, 16 μm bead). A small aliquot for subsequent analysis by SDS-PAGE was taken ("Input") and the remaining lysate was clarified by centrifuging for 10 min at 4°C and 2000 g. The supernatant was transferred to a 1.5 mL ultracentrifuge tube (Beckman-Coulter, #357448) and the membranes were pelleted at 100,000 g for 1 h at 4°C in a TLA 100.3 rotor (Beckman-Coulter). Afterward the supernatant was taken off and stored at −20°C ("S100") and the pellet was resuspended in 50 μL PBSI. A small aliquot of 25 μL was stored at −20°C for analysis by SDS-PAGE ("P100") and the remaining 25 μL were subjected to alkaline extraction by adding 75 μL of 250 mM Na_2CO_3 (pH 11) (Sigma Aldrich, #A0634292404) for 15 min on ice. The sample was transferred to a 250 μL ultracentrifuge tube (5 × 20 mm Beckman-Coulter, #342630) and a 50 μL of 10% sucrose cushion was placed below the sample at the bottom of the tube. The samples were then centrifuged for 1 h at 100,000 g and 4°C in a TLS 55 rotor (Beckman-Coulter) with the appropriate adapters (#358614). The top 200 μL were carefully taken off and stored at −20°C ("S100E") and the pellet was resuspended in 50 μL PBS and stored at −20°C ("P100E"). The samples were subsequently analyzed by SDS-PAGE and western blotting to PVDF membranes (see respective sections).

Denaturing SDS polyacrylamide gel electrophoresis (PAGE) and immunoblotting

SDS-PAGE analysis was carried out either with 10% gels (TGX FastCast acrylamide Kit 10%; Bio-Rad) or precast 4–15% gradient gels (Mini-PROTEAN TGX precast gel; Bio-Rad). The protein concentration was determined using the Pierce 660 nm protein assay (Thermo-Fisher). Samples were denatured by the addition of SDS sample buffer (62.5 mM Tris-HCl, pH 6.8, 10% glycerol, 2% SDS, 0.002% bromophenol blue, 5% β-mercaptoethanol) and boiled for 10 min at 95°C. For western blotting the proteins were transferred to polyvinylidene difluoride (PVDF) membranes using the Trans-Blot Turbo RTA Mini PVDF Transfer Kit (Bio-Rad) and the Trans-Blot Turbo Transfer System (Bio-Rad). Membranes were blocked for 1 h in 3% BSA/TBST (20 mM Tris-HCl, pH 7.4, 137 mM NaCl, 0.1% Tween 20) at room temperature. The incubation with the primary antibody was carried out in 3% BSA/TBST either for 1 h at room temperature or overnight at 4°C. After extensive washing with TBST the membranes were incubated with the secondary HRP-conjugated antibodies diluted in 5% skim milk/TBST for 1 h at room temperature. The membranes were again extensively washed with TBST and the ECL reagent (GE Healthcare) was mixed and added for 1 min afterward. Images were acquired using Vilber-Lourmat instrument and its software.

Lipid droplet flotation

One 10 cm dish of day 6 3T3-L1 adipocytes was used. The cells were washed with ice-cold PBS and subsequently harvested by scraping in PBS. The cells were centrifuged at 600 g, 4°C for 5 min. The supernatant was discarded, and the pellet containing the cells was resuspended in 1 mL PBS supplemented with protease inhibitor (cOmplete, Mini, EDTA-free Protease Inhibitor Cocktail; Merck). The cells were lysed by 20 passages through a bead homogenizer (16 μm bead, Isobiotec) and the lysate was clarified at 600 g, 4°C for 10 minutes. The supernatant was transferred to a new 1.5 mL tube and supplemented with 60% sucrose/PBS to a final concentration of 12% sucrose. 600 μL of the lysate were transferred to an ultracentrifuge tube (5 × 41 mm, Beckman-Coulter, #344090) and centrifuged in an MLS-50 rotor (Beckman-Coulter) at 100,000 g, 4°C for 1 h. After the centrifugation the tubes were sealed, and the lower boundary of the floating lipid droplet fraction was marked. The tubes were flash frozen in liquid nitrogen and the top and were collected by cutting the frozen tube. The middle fraction was collected after thawing and the remaining pelleted fraction was washed once with PBS and then resuspended in PBS. All samples were then stored at −20°C until further analysis by SDS-PAGE.

Membrane flotation

Flotation experiments were carried out using five 10 cm dishes COS7 cells. Cells were washed with ice-cold PBS and subsequently harvested by scraping in PBS. The cells were briefly pelleted at 600 g, 4°C for 5 min. The supernatant was discarded, and the pellet was resuspended in 1 mL PBS supplemented with protease inhibitor (cOmplete, Mini, EDTA-free Protease Inhibitor Cocktail; Merck). The cells were lysed by approx. 20 passages through a bead homogenizer (Isobiotec, 16 μm bead) and the lysate was cleared from debris at 600 g, 4°C for 10 min. 100 μL supernatant was collected and stored at −20°C; the remaining supernatant was transferred to a 1.5 mL ultracentrifuge tube (Beckman-Coulter) and centrifuged in a TLA 100.3 rotor (Beckman-Coulter) at 100,000 g, 4°C for 1 h. The supernatant was transferred to a new 1.5 mL tube and stored at −20°C for later analysis. The pellet was resuspended in 36 μL PBS supplemented with protease inhibitor and 10 μL were stored for later analysis at −20°C. The remaining 26 μL were supplemented with 150 μL of 60% sucrose (w/v). To remove the ribosomes from the membranes 24 μL puromycin (10 mg/mL) were added to a final concentration of 2.5 M puromycin and 45% sucrose. The reaction was incubated at RT for 30 min. 300 μL of 35% sucrose (w/v) were added to a 600 μL ultracentrifuge tube (Beckman-Coulter) and the resuspended pellet fraction in 45% sucrose (w/v) was loaded to the bottom of the tube. Finally, 150 μL of 5% sucrose (w/v) were pipetted on top, the interphases were marked, and the

sample centrifuged in an MLS 50 rotor (Beckman-Coulter) at 150,000 g, 4°C for 3 h. The tubes were subsequently frozen in liquid nitrogen and the fractions separated by cutting the tube at the interface marks using a clean scalpel. The fractions that were collected are the top fraction with 5% sucrose, the interphase between 5% and 35% sucrose, the 35% sucrose fraction, the interphase between 35% and 45% sucrose and the bottom fraction with 45% sucrose. The protein concentration of the fractions was determined, and equal amounts analyzed by SDS-PAGE.

Indirect immunofluorescence

For indirect immunofluorescence experiments cells were trypsinized and transferred either to Ø 18 mm cover glasses (No. 1; VWR) in 12-well tissue culture plates (TPP) or to 96-well plates (Greiner) and cultured using DMEM supplemented with 10% of the respective serum (calf serum CS for 3T3-L1 or FBS for COS7 and differentiated adipocytes). Differentiated adipocytes were cultured for at least two days after trypsinization to ensure proper settling of the cells. Cells were fixed with 4% paraformaldehyde (PFA; Electron Microscopy Sciences) at 37°C for 30 min. After washing three times with PBS, cells were permeabilized for 15 min either with 0.1% Triton X-100 in PBS, or, when PLIN2 or PLIN3 or 4 were stained in adipocytes, 0.2% saponin and 1% CS in PBS. Cells were again washed and incubated with primary antibodies in blocking solution (PBS supplemented with 1% CS) for 1 h at RT. After washing, the cells were incubated with fluorescently labeled secondary antibodies in blocking solution for 1 h at RT. For lipid droplet visualization HCS LipidTOX Green/Red/Deep Red dyes (Thermo-Fisher, #H34475/#H34476/3H34477, respectively) were used at 1:500 dilution in PBS. Nuclei were counterstained using DAPI (Thermo-Fisher) at a concentration of 0.4 μL/mL for 10 minutes at RT. Cell outline staining, if applied, was done using Atto 490LS NHS-Ester (ATTO-TEC) at a dilution of 1:800,000 in carbonate buffer for five minutes at RT.

Cover glasses were mounted onto Superfrost Excell glass slides (Thermo-Fisher) using Fluoromount G (SouthernBiotech). Image acquisition was performed as described under "microscopy".

Determination of protein concentration

Protein concentration was determined in 96-well plates using the Pierce 660 nm Protein Assay (Thermo-Fisher) according to the manufacturer's manual. A standard-curve was produced with a BSA solution ranging from 50 to 2000 μg/mL.

Microscopy

Confocal fluorescent microscopy was done on a Nikon Eclipse Ti-E microscope with enhanced CSU-W1 spinning disk (Microlens-enhanced dual Nipkow disk confocal scanner, wide view type), a Nikon CFI PlanApo 100x oil immersion objective (NA 1.49), and a sCMOS PCO Edge 5.5 camera (PCO, 2560x2160 pixels).

For automated confocal microscopy a Yokogawa CellVoyager 7000 spinning disk confocal microscope with enhanced CSU-X1 spinning disk (Microlens-enhanced dual Nipkow disk confocal scanner, wide view type), a 40x air objective (NA 1,15) or 60x water immersion (NA 1,2), and three *Neo* sCMOS cameras (Andor, 2560x2160 pixels) were used. 108 sites were acquired per well of a 96-well plate with seven confocal planes of 1 μm thickness per site, which were maximum intensity projected before saving. The signals for UV (405 nm) and far-red (640 nm) as well as green (488 nm) and Atto490LS (675 nm) signals were acquired in dual-camera mode. Red signal (561 nm) was acquired separately.

Images for parts of Figures 4, S4, and S2H–S2I were captured on an Olympus SpinSR10 spinning disc confocal system fitted with an Olympus IX-83 frame, a Yokogawa CSU-W1 SoRa super-resolution spinning disc module, a Photometrics Prime BSI camera and a 60× objective (1.5 NA, UPLAPOHR60x), using Olympus cellSens Dimension software. When indicated the images were post-processed using an OSR filter (standard) and deconvolved (constrained iterative, maximum likelihood, 5 iterations) using Olympus cellSens Dimension software (version 3.1.1).

Automated image analysis

The acquired images were analyzed using CellProfiler (https://cellprofiler.org/). When necessary the cell profiler pipelines were run on the high-performance cloud computing system "ScienceCloud" at the University of Zurich. Analysis pipelines were composed of generic or partially customized modules as described.[62] Individual cells were segmented with nuclei as primary objects that were identified based on DAPI signal, and cell outlines were determined from Atto490LS signal using iterative segmentation based on a watershed algorithm and related to nuclei as secondary objects. After cell segmentation the background of all stainings of interest was subtracted and single-cell based features like area, shape, intensities and textures were extracted using the modules "MeasureObjectAreaShape", "MeasureObjectIntensity", and "MeasureTexture".

Single cell classification by support vector machines (SVMs)

Single cells were classified using user supervised machine learning with a custom MATLAB script CellClassifier.[63] The classifier is based on support vector machine algorithm (SVM). In general, the classifiers were trained to identify and remove cells that were miss-segmented using nuclear area, nuclear shape, intensity, and textures as training features. Cells which overlapped with the border of an individual imaging site were automatically identified and removed. Furthermore, experiment specific SVMs were trained using intensity, channel correlation and texture as training features.

Cloning of truncations and deletion mutants

All truncation- and deletion-mutants were cloned by restriction ligation into the mEGFP-C1 using *Hind*III and *Kpn*I restriction sites. The mEGFP-C1 plasmid was a kind gift from Michael Davidson (Addgene plasmid #54759).

Cloning of GFP-PLIN2-251InsIMs

Cloning of the PLIN2 domain swap mutant carrying the core iMS (PLIN1 amino acids 238–268) of PLIN1 was done by insertion of the iMS sequence into mEGFP-C1-PLIN2 after amino acid 251 of the PLIN2 sequence. The insertion was done using the Q5 Site-Directed Mutagenesis Kit (NEB) and design of respective primers using the NEBaseChanger online tool (http://nebasechanger.neb.com/).

Generation of stable cell line for inducible expression of GFP-PLIN1

The stable 3T3-L1 cells with inducible GFP-PLIN1 or GFP-PLIN1ΔΔ (Δ238-280-Δ348–370), respective transgenes were generated by lentiviral gene transfer using the pINDUCER20 construct and Gateway cloning technology. The pInducer20 was a kind gift from Stephen Elledge (Addgene #44012). The respective transgenes were first sub-cloned by TOPO cloning into a Gateway entry vector (pENTR/D-TOPO; Thermo-Fisher) and subsequently recombined into the pINDUCER20 vector using the Gateway LR Clonase II Enzyme mix (Thermo-Fisher). Production of lentiviruses and transduction of cells was performed as described below.

The cell lines were subsequently established by selecting positively transduced cells using G418 selection (1 mg/mL) for several passages.

Expression of the respective transgene was usually induced with 500 ng/mL anhydrotetracycline (ATC) for the indicated timeframes.

Preparation of sodium oleate

To prepare a solution of sodium oleate, 30 mL of double-distilled water were warmed up in the microwave to approx. 40°C and 400 μL of 5 M NaOH were added. While constantly stirring, 400 μL of oleic acid (Sigma-Aldrich) were slowly added and the solution was stirred for another 5 min (stock concentration 41 mM). If micelles where still visible, additional NaOH was added until all micelles disappeared. The solution was sterile filtered through a 0.22 μm sterile filter, aliquoted and stored at −20°C. Using 147 μL of the solution per 25 mL of culture medium resulted in a final concentration of 250 μM.

Cell treatments

Lipolysis was induced in differentiating adipocytes by addition of 1 mM forskolin in the medium (or vehicle, DMSO) to the final concentration of 10 μM, for 6 h. Oleate uptake was done by adding sodium oleate to the medium in the indicated concentration for 6 h. Protein synthesis was inhibited by incubating cells in the medium containing cycloheximide (or DMSO control) to final concentration of 100 μg/ml for the indicated time.

Cover glasses acid wash

Cover glasses (Ø 18 mm; VWR No. 1) were placed in a ceramic rack and submerged in 2 M HCl for 15 min. The coverslips were rinsed under tap water for 30 min and then washed three times with double-distilled water. Finally, the coverslips were rinsed in ethanol, sterilized under UV-light for 30 min and stored in a closed container in a tissue culture hood.

Production of lentivirus for gene transfer

Lentivirus for gene transfer and integration of pINDUCER constructs was produced in HEK 293T cells (Dharmacon). The cells were cultured in DMEM supplemented with 10% FBS, 25 mM HEPES (Sigma-Aldrich, H4034), 1 mM sodium pyruvate (Thermo-Fisher), 2 mM glutamine (Sigma-Aldrich) and 100 μM non-essential amino acids (Thermo-Fisher) on 10 cm dishes until reaching approx. 70% confluency. The cells were transfected using the calcium phosphate method with the three components necessary for the lentiviral packaging: 10 μg of the pINDUCER expression vector containing the construct of interest, 6.5 μg psPAX2 (Addgene # 12260), the viral genome packaging plasmid, and 3.5 μg pMD2.G (Addgene # 12259), encoding for the viral envelope components were gently mixed with H_2O to a total volume of 597 μL. This was mixed with 682 μL 2x HBSS (Hank's Balanced Salt Solution), and 85 μL 2 M $CaCl_2$ were added followed by 30 min incubation at RT. The entire transfection mix was added dropwise to the cells and incubated for approx. 12 h at 37°C, 5% CO_2. After that the medium was replaced by DMEM supplemented with 5% FBS. The media containing the lentiviral particles was collected at 24, 48, and 60 h after changing the medium. The individual fractions were sterile filtered through a 0.45 μm filter, pooled and stored at 4°C. The virus particles were then concentrated to approx. 200 μL final volume using an Amicon Ultra-15 centrifugal filter unit (Merck) with a molecular weight cut-off of 100 kDa (Amicon "Ultra – 15 centrifugal filter"; 100 kDa MW-cut off). The filtrate was brought to 1 mL final volume with DMEM supplemented with 10% CS and immediately used for transduction of 3T3-L1 cells as described below.

Transduction of 3T3-L1 preadipocytes with lentivirus

3T3-L1 cells were grown in 6-well plates until 50–60% confluency before the medium was replaced by the concentrated virus mixture supplemented with 8 μg/mL polybrene (Sigma-Aldrich, #107689). After overnight incubation the medium was replaced by DMEM supplemented with 10% CS. Cells were further selected or subjected to single clone dilution as described below.

In vitro experiments

The purification protocol for LDs from cells expressing fluorescently tagged LD proteins was the same as in Ajjaji et al. 2019. Briefly, cells from 5 × 15 cm dishes were harvested, washed once in ice-cold PBS, and lysed using a 30G needle in 1 mL 20 mM Tris-EDTA buffer containing complete protease and phosphatase inhibitor tablets at pH 7.5. To isolate LDs, 1 mL of respective cell lysates were mixed with 1 mL 60% sucrose in 20 mM Tris-EDTA buffer supplemented with protease inhibitors, overlaid with 20%, 10% and 0% in buffered sucrose on top of one another in 5 mL Ultra-Clear centrifuge tubes (Beckman). Gradients were centrifuged for 16 h at 100,000 x *g* and 4°C, using an SW60 rotor in a Beckman L8-70 centrifuge, and 300 μL were collected from the top as the LD fraction.

In vitro experiments were performed in HKM buffer: 50 mM HEPES, 120 mM K^+OAc, and 1 mM $MgCl_2$ (in Milli-Q water) at pH 7.4. To create buffer-in-oil drops, a buffer-diluted LD fraction was mixed with an excess of triolein by vortexing, as previously done in Ajjaji et al. 2019. The shrinkage of the buffer compartment was based on water evaporation of the aqueous drops, with the proteins at their surface, during imaging for 10 to 15 min on PDMS-coated glass slides.

Fluorescence recovery after photo bleaching FRAP experiments

For FRAP experiments, we bleach the signal on a collection of drops and monitor the signal recovery. The background signal, e.g., from the cytosol, is removed from the recorded signal, which was at the end normalized by intrinsic bleaching of non-bleached areas. We used GraphPad Prism to fit the FRAP recovery curves with a non-linear regression and the exponential « one-phase association model ». The characteristic recovery time is extracted from the model. When indicated Huh7 cells (60–70% confluence) were exposed for 1hr to 500 μM oleic acid coupled to BSA (1% v/v) to induce LD formation and then cells were transfected with 3 μg of plasmid DNA/mL using Polyethylenimine HCl MAX (Polysciences, Inc) following the manufacturer's instructions.

QUANTIFICATION AND STATISTICAL ANALYSIS

Number of samples and replicates in an experiment, as well as dispersion (standard deviation, SD, standard error of the mean, SEM), are reported for each figure in the respective legends. Quantification of experimental data are described in relevant STAR methods sections.